


Review

Imaging Key Biomarkers of Tumor Angiogenesis

Marina V. Backer, Joseph M. Backer 

SibTech, Inc. Brookfield, CT 06804, USA.

 Corresponding author: Joseph M. Backer, Tel: +1-203-775-5677, Fax: +1-203-775-5705, e-mail: jbacker@sibtech.com.

© Ivyspring International Publisher. This is an open-access article distributed under the terms of the Creative Commons License (<http://creativecommons.org/licenses/by-nc-nd/3.0/>). Reproduction is permitted for personal, noncommercial use, provided that the article is in whole, unmodified, and properly cited.

Received: 2011.10.11; Accepted: 2012.01.07; Published: 2012.05.17

Abstract

Angiogenesis is a fundamental requirement for tumor growth and therefore it is a primary target for anti-cancer therapy. Molecular imaging of angiogenesis may provide novel opportunities for early diagnostic and for image-guided optimization and management of therapeutic regimens. Here we reviewed the advances in targeted imaging of key biomarkers of tumor angiogenesis, integrins and receptors for vascular endothelial growth factor (VEGF). Tracers for targeted imaging of these biomarkers in different imaging modalities are now reasonably well-developed and PET tracers for integrin imaging are currently in clinical trials. Molecular imaging of longitudinal responses to anti-angiogenic therapy in model tumor systems revealed a complex pattern of changes in targeted tracer accumulation in tumor, which reflects drug-induced tumor regression followed by vascular rebound. Further work will define the competitiveness of targeted imaging of key angiogenesis markers for early diagnostic and image-guided therapy.

Key words: tumor angiogenesis, molecular imaging, integrins, VEGF receptors, anti-angiogenic therapy.

Introduction

This article is intended as a review of recent advances in molecular imaging of key biomarkers of tumor angiogenesis and their responses to anti-angiogenic therapy. Although tumor neovascularization combines two distinct processes, angiogenesis and vasculogenesis, the term “angiogenesis” is often used interchangeably with the term “neovascularization” (1, 2). Under normal circumstances, neovascularization occurs during embryonic development, wound healing, and development of the corpus luteum. However, neovascularization takes place in a large number of pathologies, such as solid tumor growth, various eye diseases, chronic inflammatory states including development of atherosclerotic plaques, and ischemic injuries (3).

To focus on oncology, angiogenesis is an early hallmark of tumor growth and therefore molecular

imaging of angiogenesis is expected to help in early diagnosis of primary tumor and emerging metastatic lesions. On the other hand, recognition that inhibition of neovascularization may delay progression and perhaps even starve tumor to death resulted in enormous research and drug development efforts by countless academic and industrial groups. As a result of these efforts, several therapeutic agents, commonly known as anti-angiogenic drugs, have been approved for clinical use and hundreds of late-stage clinical trials of anti-angiogenic drugs and combination regimens are currently in progress (1-9). Unfortunately, the approved anti-cancer anti-angiogenic drugs bevacizumab (Avastin, Genentech/Roche), sunitinib (Sutent, Pfizer), sorafenib (Nexavar, Bayer), pazopanib (Votrient, GlaxoSmithKline) as well as many exploratory drugs, are effective only in relatively

small and unpredictable subsets of patients, while treatment can result in serious side effects (1-9). These shortcomings, as well as very high cost of anti-angiogenic drugs (\$50-100K/patient/year), prevent their broad acceptance by regulatory authorities and by private and national insurance providers. Therefore, there is an urgent need in imaging-based methodologies that can early and reliably identify responders and could be used for image-guided optimization and “personalization” of anti-angiogenic regimens.

Key biomarkers for imaging angiogenesis

Research in the last few decades established significant differences in organization and molecular composition of angiogenic tumor *vs.* quiescent normal vasculature. Several proteins are expressed at higher levels on the surface of endothelial cells in angiogenic vasculature and might serve as suitable targets for imaging. Importantly, unlike biomarkers on tumor cells, these targets are accessible directly from the bloodstream and therefore they can be imaged with-

out problems associated with tracer extravasation and tumor penetration. One group of angiogenic biomarkers is integrins, particularly $\alpha\beta3$ and $\alpha\beta5$ integrins. Integrins are transmembrane proteins involved in cell growth, survival, adhesion, and motility, serving as receptors for proteins in extracellular matrix (ECM) and certain immunoglobulin superfamily proteins (10-12, Fig. 1). However, in addition to endothelial cells in angiogenic vasculature, integrins are also expressed on many tumor cells, and this should be taken into account in interpretation of any integrin-related experimental results. There are twenty four $\alpha\beta$ heterodimeric integrins formed by eighteen α and eight β subunits; many integrins recognize certain exposed peptide sequences. One example is RGD (arginine-glycine-aspartic acid) that is present in many ECM and some secreted proteins, such as fibronectin, vitronectin, fibrinogen, laminin, collagen, Von Willebrand factor, osteopontin, and thrombospondin.

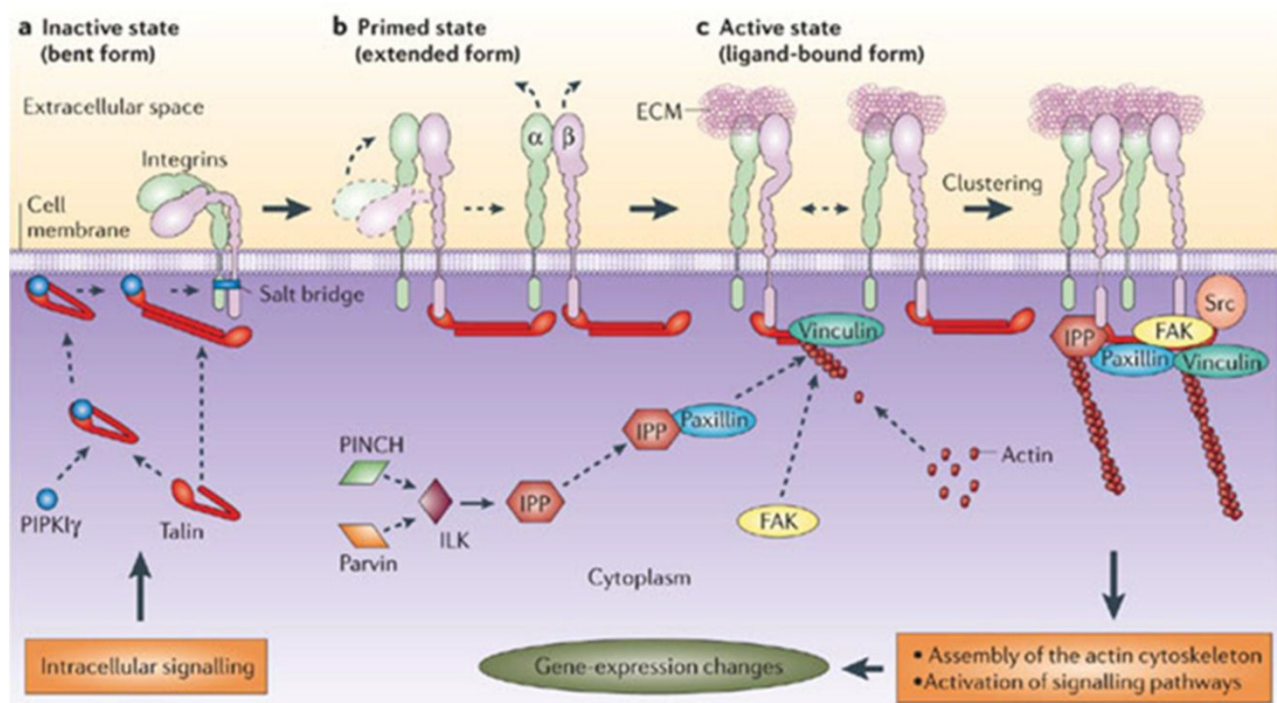


Figure 1. Integrins assemble in focal adhesions (a-c) and ‘integrate’ signals from the extracellular matrix (ECM) to the intracellular cytoskeleton (11). Many integrins that are not bound to the extracellular matrix (ECM) are present on the cell surface in an inactive conformation (a). Recruitment of intracellular proteins induces conformational transition in integrins (b), which unmask the ligand-binding site, allowing the integrin to bind specific ECM molecules (c). The maturation of focal adhesions involves clustering of active, ligand-bound integrins and the assembly of a multiprotein complex that is capable of linking integrins to the actin cytoskeleton and communicating with signalling pathways.

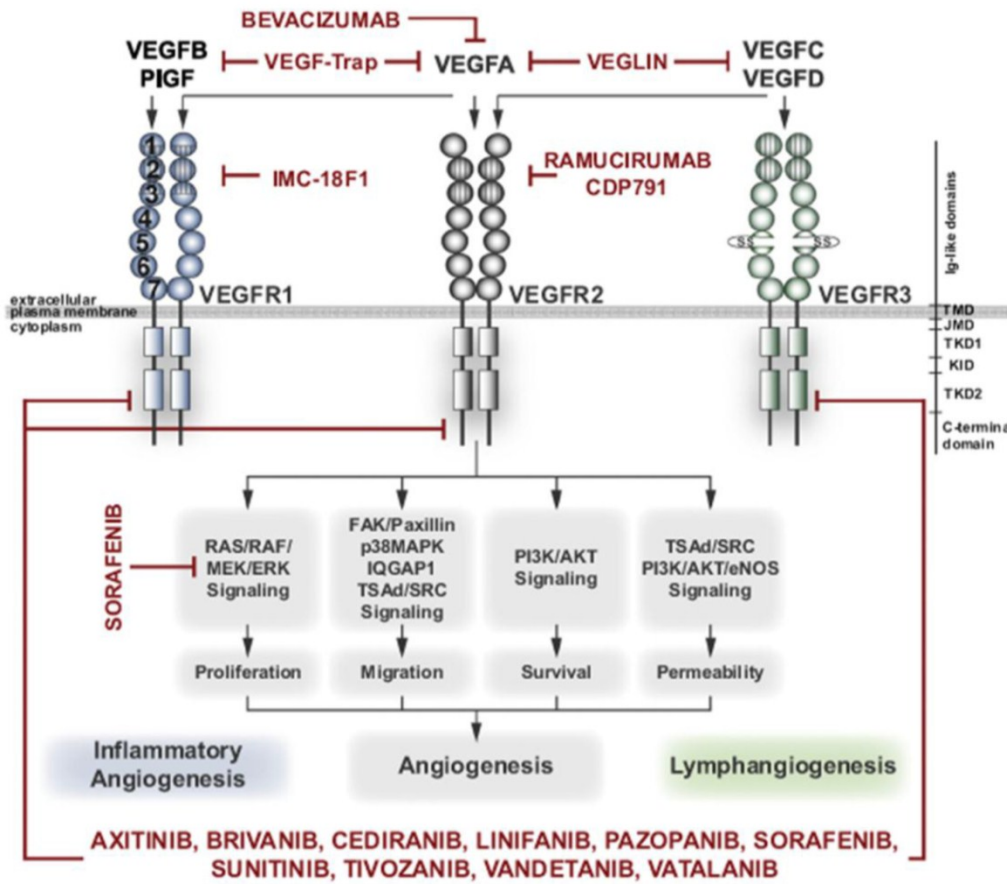


Figure 2. VEGF signaling inhibitors and their targets (13). The VEGF family of ligands (VEGFA, PIGF, VEGFB, VEGFC, and VEGFD) bind to their cognate receptors (VEGFR1; blue, VEGFR2; grey, VEGFR3; green) as indicated (arrows). Several different VEGF antagonists interfere with binding of VEGF ligands on the extracellular domain (Bevacizumab, VEGF-Trap, Veglin, IMC-18F1, Ramucirumab/CDP791), or compete for ATP-binding to the intracellular kinase domain (axitinib, brivanib, cediranib, linifanib, pazopanib, sorafenib, sunitinib, tivozanib, vandetanib, vatalanib). VEGFRs are shown with their extracellular domain organized in immunoglobulin-like loops (circles, labeled 1–7) and with intracellular split tyrosine kinase domain (squares). VEGFR1 is critical in inflammatory angiogenesis and VEGFR3 in lymphangiogenesis. VEGFR2 transduces signals to proliferation, migration, survival and vascular permeability (through pathways indicated in boxes) resulting in angiogenesis.

Interaction of integrins with RGD, or other ligands, induces assembly of signaling complexes, which promote various changes in cellular behavior (Fig. 1). Although several drugs targeting integrins are currently in clinical trials, the role of integrins in regulating angiogenesis is not yet fully understood; it is complex- and, apparently, context-dependent (10-12). However, enhanced expression of $\alpha v \beta 3$ and $\alpha v \beta 5$ integrins in tumor vasculature, as well as multiple avenues for engineering and optimization of RGD-based tracers for different imaging modalities provided a very strong impetus for developing integrin-targeting tracers for molecular imaging.

Another group of biomarkers overexpressed in tumor vasculature is the receptors for vascular endothelial growth factor (VEGF). VEGF is the crucial regulator of angiogenesis; and its action on endothelial cells is mediated by two tyrosine kinase receptors,

VEGFR-1 and VEGFR-2, primarily VEGFR-2 (13-15) (Fig. 2). VEGFR-2 is expressed predominantly on endothelial cells, although it may be also present on other cells. Immunohistochemical analysis indicates that a subset of endothelial cells at the sites of angiogenesis, particularly in the tumor growth areas, express significantly higher levels of VEGFR-2 than quiescent endothelial cells, making it a highly suitable target for diagnostic molecular imaging.

Because of its profound physiological significance, the VEGF/VEGFR pathway is the major target for anti-angiogenic drugs. The first blockbuster drugs targeting VEGFR have already been approved by FDA for treatment of several cancers with ~275,000 new US cases per year (8-9). The potential of these drugs is enormous, as judged by several hundreds of US-registered Phase III clinical trials (www.clinicaltrials.gov) for all major cancers with

annual 12 million new cases, worldwide. However, as indicated above, responses of individual patients to anti-angiogenic drugs and combination therapies are complex and unpredictable (3-9). In this respect, monitoring the prevalence of VEGF receptors in response to VEGF/VEGFR targeting drugs might be useful for treatment regimen optimization.

In addition to integrins and VEGF receptors, several other proteins are selectively overexpressed in tumor vasculature, such as matrix metalloproteinases (MMPs), prostate-specific membrane antigen (PSMA), endoglin (CD105), endosialin (CD248/TEM1), E-selectin, components of ECM, such as extra domain B of fibronectin and extra domain C of tenascin (16). Furthermore, the use of high throughput experimental methods, as well as powerful bioinformatic methods, suggest that other targets could be discovered and exploited as imaging biomarkers (17).

Molecular tracers for imaging key biomarkers of angiogenesis

Development of RGD-based tracers for imaging integrins. The first RGD-based tracers, cyclo(-Arg-Gly-Asp-D-Tyr-Val-) and cyclo(-Arg-Gly-Asp-D-Phe-Tyr-) that utilized cyclized RGD-based peptides radiolabeled with ^{125}I have been described in 1999 (18). These tracers were used for imaging integrins in three different tumor models (melanoma M21 or mammary carcinoma MaCaF in nude mice and osteosarcoma in BALB/c mice). Since that time, almost 300 publications described continuous improvement in tracer design for every imaging modality and expansion of its field of use. One key advance was introduction of polyethyleneglycol, sugar, or hydrophilic amino acid residues in the RGD-based tracers to improve pharmacokinetics, to provide facile opportunities for direct radiohalogenation, particularly with ^{18}F , or conjugation of chelators for loading with various radionuclides (12), or preparation of RGD-driven nano- and microparticle for multimodal imaging and drug delivery. As a result of these chemical advances, RGD-based tracers for PET, SPECT, MRI, fluorescent optical imaging, ultrasound imaging, and photoacoustic imaging were developed and validated in animal models (12, 19-22). Another key advance was multimerization of several copies of RGD sequences in a single construct in order to increase the affinity of the tracers to targeted cells and enhance integrin-mediated internalization (23-29). Particularly promising is recent development of various RGD-driven multimodality nano- and microparticles combining, for example, MRI and fluorescent contrast agents (30-35), or combining contrast agents and drugs (36-39). It should be noted that most pub-

lished reports describe the kinetic of clearance of RGD-based tracers from tumor and other organs, not the kinetics of accumulation. Detailed kinetic analysis of biodistribution and clearance with ^{64}Cu -RGD tracer indicates that it was cell surface binding, rather than cellular internalization that led to accumulation of tracer at early time points (40). Nevertheless, prolonged kinetics of intracellular accumulation of RGD-tracers, at least for tumors that express RGD-binding integrins on tumor cells, was demonstrated with fluorescent probes that are unquenched only in intracellular environment (34, 41). As judged by accumulation of RGD-based tracers in tumor, they successfully compete with endogenous integrin ligands. However, their accumulation in the tumor might be modulated not only by the prevalence of integrins on endothelial or tumor cells, but also by the changes in prevalence of multiple RGD-containing ligands. In general, RGD-based tracers are considered safe; however, in at least one publication, evidence of tumor-promoting activity of tracer amount of RGD-containing constructs was reported (42).

Integrin imaging and therapy monitoring. So far, there are only few publications that describe the use of RGD-driven contrast agents for monitoring anti-cancer chemotherapy. Jung et al (43) reported the use of a SPECT tracer glucosamino $^{99\text{m}}\text{Tc}$ -D-c(RGDfK) for monitoring the effects of paclitaxel treatment in two murine subcutaneous tumor models, RR1022 rat fibrosarcoma in Balb/c nude mice and mouse Lewis lung carcinoma (LLC) in C57BL6 mice. Intraperitoneal paclitaxel therapy (40 mg/kg a total of 6 doses at 2-day intervals) caused statistically significant inhibition of tumor growth and ~30% decrease in tracer uptake, however a positive correlation between tracer uptake and αv integrin prevalence in tumor was not particularly strong ($r=0.44$, $p<0.05$).

Palmowski et al (44) monitored the effects of the potent MMP inhibitor AG3340 (Prinomastat) in a model of subcutaneous human squamous cell carcinoma HaCaT-ras-A-5RT3. Microbubbles targeted by either RGD or anti-VEGFR-2 antibody reliably detected the dynamics of both $\beta 3$ integrin and VEGFR-2 in the course of AG3340 therapy (150 mg/kg i.p., twice a day for 7 days). In agreement with immunohistochemical data, the uptake of targeted microbubbles in treated animals was lower than in contemporary control mice, but was not statistically significantly affected when analyzed longitudinally, relative to the uptake at the beginning of treatment. Interestingly, the same group reported that subcutaneous AT-1 prostate cancers in rats treated with carbon ions (16 Gy) displayed significantly higher binding of integrin-targeting microbubbles and upregulation of

integrin expression without significant changes in microvascular density (45).

GE Healthcare group reported the use of ^{18}F -AH111585 (fluciclatide) cyclic RGD-based PET tracer (currently in clinical trials) for evaluation of responses to two specific anti-angiogenic drugs, VEGFR-2 tyrosine kinase inhibitors ZD4190 and sunitinib (46-48). Longitudinal imaging of nude mice bearing subcutaneous human lung adenocarcinoma Calu-6 indicated that three days of treatment with ZD4190 (100 mg/kg orally daily) did not affect tumor growth, but uptake of fluciclatide in individual mice decreased $31.8\% \pm 4.6\%$, relative to baseline pre-treatment uptake (in %ID/g) in the same animal ($n = 10$) (Fig. 3). In contrast, uptake of the tracers in control animals was increased by $26.9\% \pm 9.4\%$, suggesting that ZD4190 causes changes in tracer uptake (46). However, there were no changes in the microvascular density in ZD4190-treated vs. control mice, as measured by CD31 immunostaining. Furthermore, treatment of LLC tumor grown in C57BL/6 mice with paclitaxel (10 mg/kg i.p. daily, for 4 days) caused a $\sim 35\%$ decrease in average fluciclatide uptake in treated vs control mice also without changes in the

microvascular density.

Longitudinal imaging of mice bearing subcutaneous U87 MG human glioblastoma-astrocytoma tumors treated with sunitinib (60 mg/kg orally daily, two 5-day cycles with 2-day no drugs between cycles) also indicated a small but significant decrease in fluciclatide uptake (13-17%), relative to the baseline pre-treatment level observed from Day 2 to Day 9 of treatment (47). In contrast, in control animals there was a small but significant increase in tracer uptake relative to the baseline level. It should be noted that longitudinal imaging was particularly instrumental in this system, because control tumors grew rapidly and developed a necrotic core with tracer uptake concentrated in the outer rim of tumor, while tumor growth in treated animals was slow and tracer uptake was observed throughout the tumor. It should be noted, however, that in sunitinib-treated animals the decrease in tumor microvascular density by Day 13 was far more dramatic, $\sim 73\%$ relative to control tumors than the changes in tracer uptake. However, considering the different patterns of tracer uptake in control and treated tumors, these discrepancies are not particularly surprising.

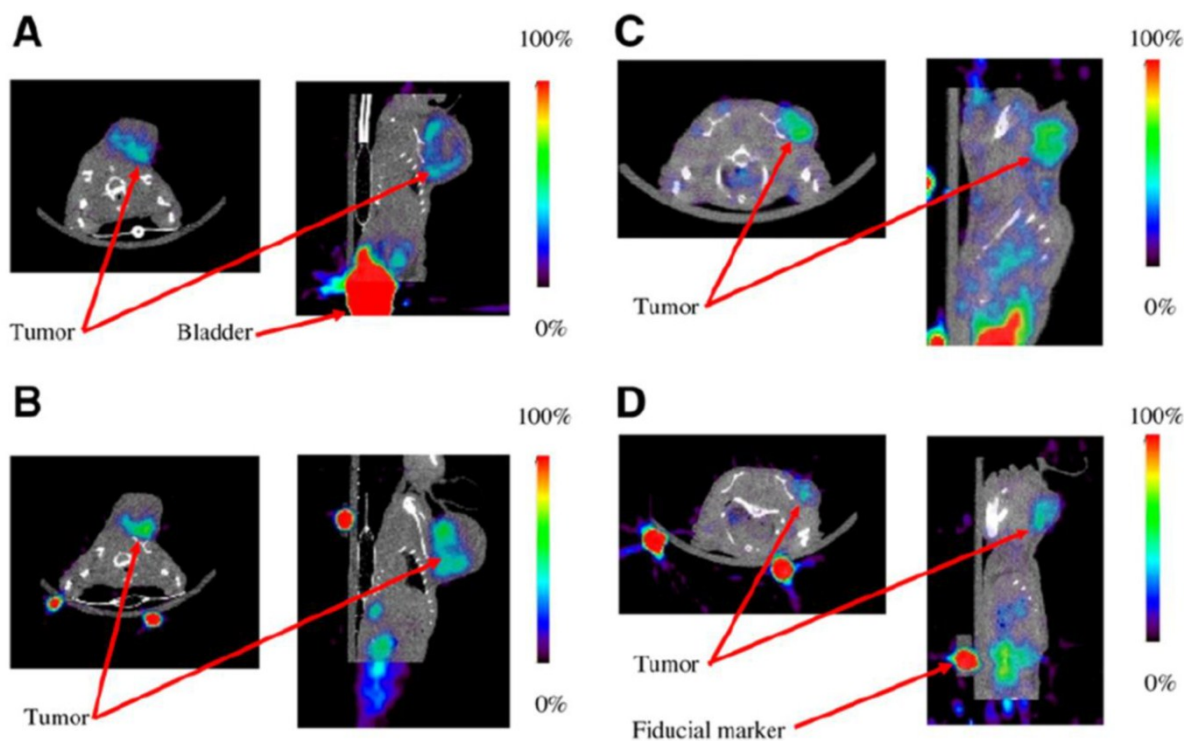


Figure 3. Representative coregistered small-animal PET and micro-CT images demonstrating ^{18}F -AH111585 uptake at 120 min in Calu-6 xenograft model before (A) and after (B) administration of 3 doses of vehicle control or before (C) and after (D) 3 doses of 100 mg/kg of ZD4190 (46). Contrast is clearly seen in Calu-6 tumors located on left shoulder region in both ZD4190-treated and vehicle control animals. The only additional higher activity concentration was found in bladder. In addition, ^{22}Na fiducial markers can be seen located on base of imaging bed (used for PET/CT coregistration). ROI analysis for tumor uptake before ZD4190 therapy was 1.7 %ID/g, decreasing to 1.1 %ID/g after ZD4190 therapy. Muscle uptake was maintained at 0.5 %ID/g in pre and post-ZD4190-therapy images. For animals treated with vehicle control alone, ROI analysis for tumor uptake before vehicle control was 2.1 %ID/g, increasing to 2.5 %ID/g after therapy. Muscle uptake was maintained at 0.3 %ID/g in pre- and posttherapy images.

Dumont et al (49) reported the use of [^{64}Cu]DOTA-cyclo-(Arg-Gly-Asp-DPhe-Lys) PET tracer for evaluation of the dasatinib, an inhibitor of Src family and other tyrosine kinases, which is currently undergoing multiple clinical trials. This group used the same U87 MG tumor model and validated the drug activity by a decrease in immunostaining for phospho-FAK. After three days of treatment (72 or 95 mg/kg orally daily), RGD tracer uptake in treated animals vs. control was decreased by 39% in the 72 mg/kg dose group and 59% in the 95 mg/kg dose group. However, tumor growth, ^{18}F -FDG uptake, the levels of vascularization (as judged by CD31 staining), and $\alpha\text{v}\beta 3$ levels were not affected at that time, making interpretation of the changes in tracer uptake rather difficult.

Finally, Yang et al (50) used ^{18}F -FPPRGD2 (2-fluoropropionyl labeled PEGylated dimeric RGD peptide [PEG3-E{c(RGDyk)}₂]) PET tracer to evaluate responses to 3-day treatment with ZD4190 (100 mg/kg, daily, orally) in human MDA-MB-435 tumor grown in nude mouse fat pad. It should be noted that for many years MDA-MB-435 were considered to be derived from human breast carcinoma, but recent analyses indicated that currently available cells are, most likely, derivative of human M14 melanoma cell line (see, <http://www.lgcstandards-atcc.org/MisidentifiedCellLines/tabid/1171/Default.aspx>). In MDA-MB-435 model, unlike in Calu-6 tumors (46), a 3-day treatment with ZD4190 virtually blocked tumor growth for 7 days, after which tumor growth resumed with the rate similar to that in control animals. Somewhat surprisingly, PET imaging with ^{18}F -FDG indicated that glucose metabolism was not affected by tumor growth inhibition, while PET imaging with ^{18}F -FLT indicated that cell proliferation was inhibited on Day 1 and 3, but returned to the pre-treatment baseline by Day 7. The longitudinal changes in the uptake of ^{18}F -FPPRGD2 PET tracer displayed a similar pattern, a decrease of ~17.5% and 28.5% relative to the pretreatment baseline on Day 1 and 3, and return to the baseline at Day 7. Interestingly, expression of human $\alpha\text{v}\beta 3$ integrins on MDA-MB-435 appears to be decreased by ~30% and 46% on Day 1 and 3 of the treatment but return to the baseline by Day 7. Taken together, the initial experience with RGD-based tracers for monitoring chemotherapy in animal tumor models indicates that it is possible to detect small but significant drug-induced decreases in tracer uptake. However, the connections between timing and magnitude of these changes and alterations in tumor vasculature appears to be system- and drug-dependent, reflecting drug-induced complex changes in integrin prevalence, internalization, and

occupancy by host ligands. Obviously, further research is necessary to untangle these processes and assess their effects on longitudinal changes in integrin imaging with RGD-based tracers.

Clinical trials with RGD-based tracers. To date, several clinical trials with RGD-based tracers are either completed or in progress. ^{18}F -galacto-RGD PET tracer was tested in cancer patients (51-58). The tracer is safe with an overall patient exposure similar to that from ^{18}F -FDG imaging. ^{18}F -galacto-RGD PET uptake was highly variable between patients and between different tumor lesions in the same patient, as well as highly heterogeneous within individual lesions. Importantly, ^{18}F -galacto-RGD readily accumulated in many, but not all lesions that were identified by other imaging modalities. Some lesions negative for ^{18}F -galacto-RGD uptake were confirmed to be negative for $\alpha\text{v}\beta 3$ presence. Interestingly, there was a poor correlation between ^{18}F -FDG and ^{18}F -galacto-RGD uptake in individual lesions, suggesting that each tracer can provide independent information for staging and molecular analysis of tumor lesions.

Several reports described the use of RGD-based $^{99\text{m}}\text{Tc}$ -NC100692 tracer developed by GE Healthcare for detection of primary breast cancer lesions (59, 60) and metastatic lesions in patients with lung or breast cancer (61). The tracer was safe and well tolerated. Scintigraphy with $^{99\text{m}}\text{Tc}$ -NC100692 identified 19 out of 22 primary lesions (86%), which range in size from 5 mm to 40 mm. Importantly, six benign lesions were not identified with $^{99\text{m}}\text{Tc}$ -NC100692, whereas fine benign changes, 4 fibrocystic changes and 1 infected cyst, were identified. However, only infected cyst displayed focal accumulation of tracer similar to that in malignant lesions, while uptake in fibrocystotic lesions was diffused, not focal, and readily distinguished from malignant lesions. In addition, imaging of axillary region detected lymph node metastases >20 mm, but not small <5 mm non-palpable ones. Screening for metastatic lesions in breast cancer patients (n=10) $^{99\text{m}}\text{Tc}$ -NC100692 scintigraphy detected 1 of 7 liver, 4 of 5 lung, 8 of 17 bone, and 1 of 1 brain metastases. Screening for metastatic lesions in lung cancer patients were 0 of 2 liver, 17 of 18 lung, 2 of 2 bone, and 7 of 9 brain metastases. Authors concluded that $^{99\text{m}}\text{Tc}$ -NC100692 scintigraphy could be useful for detection of lung and brain metastases, but not bone and liver metastases.

Imaging with ^{18}F -AH111585 (fluciclatide) PET tracer (62) was used in 7 patients with metastatic breast cancer (3 patients with metastases only in the liver, 2 with metastases only in the lung, 1 with metastases only in bone and 1 with metastases in bone and a supraclavicular lymph node). In these patients

PET imaging identified all 18 lesions that were detected by CT (Fig. 4). Interestingly, PEGylated fluciclatide accumulated in lesions gradually, reaching a plateau by 50-60 min and displaying apparently irreversible binding to its target. In contrast, ^{18}F -galacto-RGD accumulated faster but binding appears to be reversible (55).

Finally, a group from Stanford University described the results of a pilot study of ^{18}F -FPPRGD2 PET (2-fluoropropionyl labeled PEGylated dimeric RGD peptide [PEG3-E{c(RGDyk)}2]) PET tracer in healthy volunteers and reported favorable dosimetry and pharmacokinetics for this tracer (63).

Taken together, these initial clinical studies established that RGD-based nuclear tracers are safe and can be used for detection of primary and metastatic lesions. Further studies will indicate whether and under what circumstances these molecular tracers are superior to other diagnostic imaging procedures and

whether they can be used for image-guided therapy with anti-angiogenic or other therapeutic regimens.

Development of tracers for imaging VEGF receptors. Several types of targeting moieties are currently used for development of tracers for imaging VEGF receptors in angiogenic vasculature: various versions of human VEGF itself, anti-VEGFR antibody, VEGFR-binding peptides, and small molecule compounds. The VEGF-based tracers are particularly attractive for potential clinical development because they are expected to be less immunogenic and are rapidly internalized via VEGF-induced VEGFR-mediated endocytosis, providing for intracellular tracer accumulation. On the other hand, unless specifically re-engineered, VEGF-based tracers would bind to both VEGFR-1 and VEGFR-2, and also there is a risk of affecting host vasculature, even at low concentrations of VEGF.

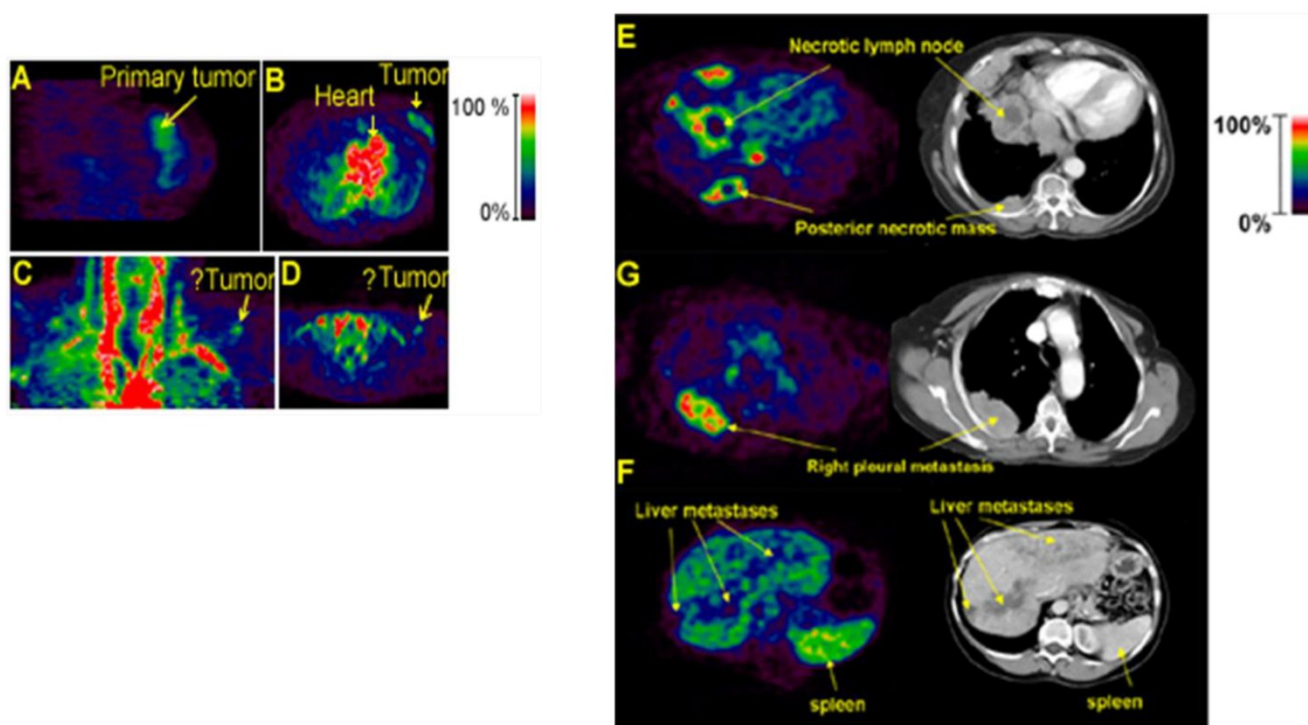


Figure 4. PET imaging with ^{18}F -AH11585 in cancer patients (62). Left Panel, PET images showing localization of ^{18}F -AH11585 in patient 2 with grade II invasive ductal breast carcinoma in sagittal (A) and transverse (B) views. PET images of patient 1 with SCF in coronal (C) and transverse (D) views. Right Panel, ^{18}F -AH11585 PET of metastatic lesions and corresponding CT images showing increased signal in periphery of lesions in patient with lung and pleural metastases (E), intralesion heterogeneity of uptake within pleural metastasis in PET image, which was not demonstrated as necrosis on corresponding CT section (G), and liver metastases imaged as hypointense lesions because of high background signal (F). High uptake in spleen is possibly due to blood pooling. See also color bar for PET images.

Three groups reported on iodination of recombinant VEGF₁₂₁ and VEGF₁₆₅ with ¹²³I or ¹²⁵I and the use of these tracers in mouse tumor models (64, 65) and even in human patients in Europe (66, 67). However, uncertain VEGF functional activity, potential dehalogenation of radioactive iodine, and a very high liver uptake (44 %ID/g and 32 %ID/g, respectively) made further development of these iodinated tracers highly unlikely. Several ⁶⁴Cu PET tracers based on His-tagged recombinant VEGF₁₂₁, which was randomly derivatized with DOTA on lysine residues, have been developed at Stanford University and used for imaging VEGF receptors in angiogenic vasculature in tumor and ischemia models (68-72). This group also described a VEGF-driven multimodality tracer based on DOTA-derivatized quantum dots randomly conjugated to VEGF enabling both PET and near-infrared imaging (73).

Since VEGF₁₂₁ is a dimeric protein with 14 lysine residues, random conjugation of radionuclide chelators inevitably generates a mixture of tracers with different properties. To avoid these problems, several VEGF-based tracers designed for site-specific conjugation of contrast agents or radionuclide chelators have been described in the last few years. Two groups used ¹¹¹In for site-specific radiolabeling of either VEGF₁₂₁ with DTPA conjugated to Cys-116 or transferring moiety in transferin-VEGF₁₆₅ fusion protein (74, 75). VEGF₁₂₁ was expressed with Avi-tag for site-specific biotinylation followed by coupling to

streptavidin-IRDye800 for near-infrared fluorescent imaging (76).

Several site-specifically derivatized VEGF-based tracers were developed using dimeric VEGF₁₂₁ (77, 78) or a more robust and versatile single-chain VEGF derivative, named scVEGF (79). ScVEGF (Fig. 5, Left Panel) is composed of two fused 3-112 amino acid (aa) VEGF fragments, lacking a C-terminal pro-angiogenic domain, and is expressed with an N-terminal 15-aa cysteine-containing tag (Cys-tag) for site-specific conjugation of various payloads (80). Cys-tagged scVEGF was site-specifically derivatized with a PEGylated chelator DOTA for PET imaging with ⁶⁴Cu (79) and ⁶⁸Ga (81, 82), ^{99m}Tc chelator HYNIC (succinimidyl 6-hydrazinopyridine-3-carboxylate hydrochloride), it was directly radiolabeled with ^{99m}Tc for SPECT imaging (78, 79, 83), or near-infrared fluorescent dyes for fluorescent imaging (77, 79), and coupled with microbubbles for ultrasound imaging (84). Advantageously, site-specific conjugation of even large payloads (e.g., PEGylated chelators, liposomes, dendrimers) did not affect the affinity of scVEGF to VEGF receptors, VEGFR-mediated internalization of scVEGF-based conjugates, and a long-term (at least 7 days, Fig. 6, Right Panel) retention of delivered fluorescent dyes (80, 85, 86). Furthermore, recent experiments indicated that scVEGF-PEG-DOTA conjugates do not stimulate tumor growth even at cumulative doses that are at least an order of magnitude higher than those needed for imaging (87).

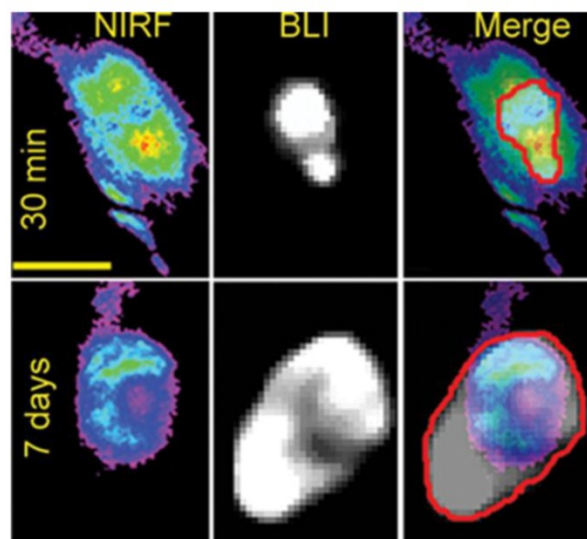
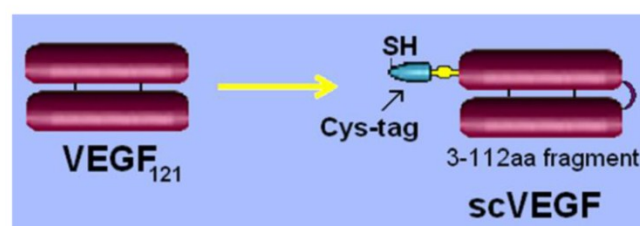


Figure 5. Imaging VEGF receptors with scVEGF-based tracers (79). **Left Panel**, Targeting protein, scVEGF was engineered by head-to-tail fusion of two 3-112 fragments of VEGF₁₂₁ and expressed with N-terminal Cys-tag for site-specific conjugation of imaging and therapeutic payloads. **Right Panel**, Long-term retention of Cy5.5 after imaging with scVEGF/Cy. 4T1 luc tumor-bearing mice (n=5) were injected with scVEGF/Cy and imaged daily for 7 days. Fresh luciferin was injected prior to each imaging. Representative first (30 min post-injection) and last (7 days post-injection) NIRF and BLI images for the same mouse are presented. On merged BLI and NIRF images the BLI footprint is contoured in red. Note that despite an average 4.5-fold increase in the tumor size, as judged by caliper measurements (from 6 × 5 × 2 mm (length × width × height) to 11 × 7 × 3 mm, average measurements) and BLI footprints, the intensity and the NIRF image area did not change significantly (ROI area ~110,000 px, ROI intensity ~280,000). Scale bar, 1 cm.

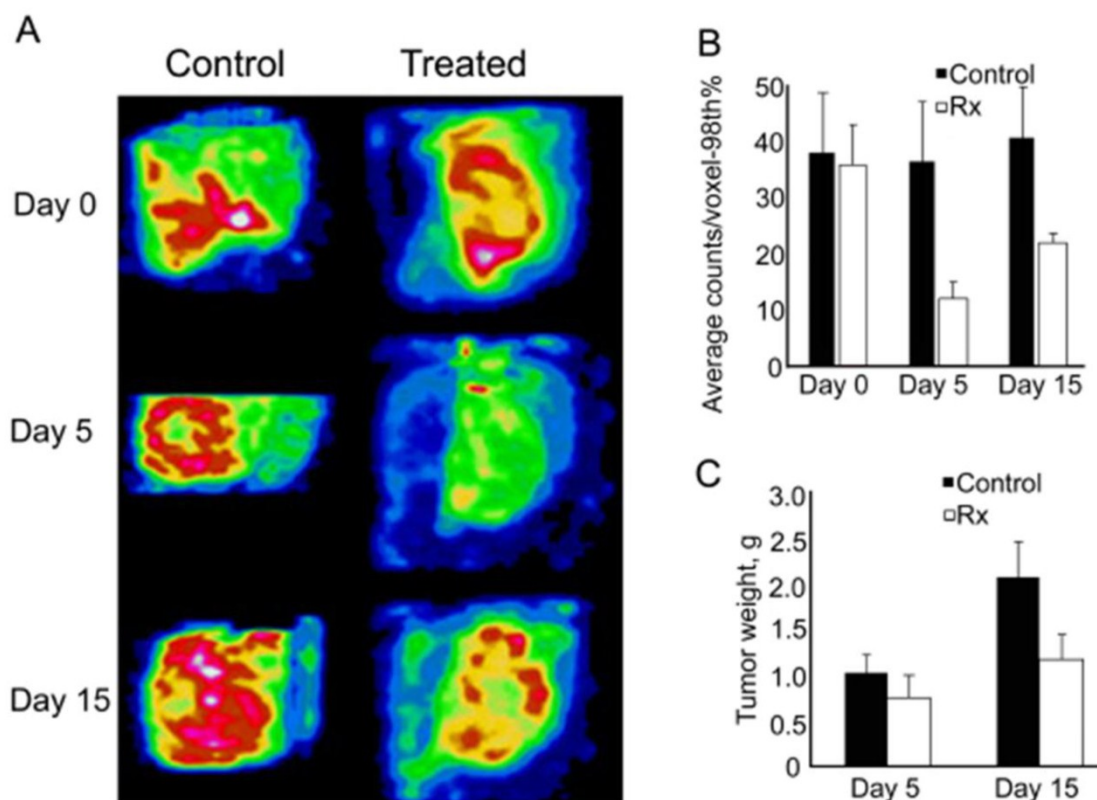


Figure 6. Pazopanib treatment affects scVEGF/^{99m}Tc tracer uptake (85). **A**, Representative anterior oblique views of the tumors from control and treated mice reconstructed from 3-D data sets obtained in serial SPECT imaging. **B**, Pazopanib significantly affects tracer uptake in areas of maximal activity. The average activity of the upper 98th percentile of voxels (98th%) was calculated from the longitudinal SPECT imaging for each mouse on Day 0, 5 and 15 for treated and timed cohorts of control mice. **C**, Tumor weights for control and treated mice. **Control**, untreated mice. **Rx**, pazopanib-treated mice.

Finally, although most VEGF-based tracers utilized VEGF-A isoforms (VEGF₁₂₁ or VEGF₁₆₅), recently, rat VEGF-C was randomly derivatized with HYNIC, radiolabeled with ^{99m}Tc, and used for imaging VEGFR-2 and VEGFR-3 in U-251 rat glioma model (88). VEGF-based tracers are internalized via VEGFR-mediated endocytosis, as judged by accumulation and persistence of fluorescent dyes in VEGFR-positive endothelial cell after injection of VEGF-based fluorescent tracers in vitro and in vivo (79, 85, 86). Recent PET kinetic experiments with scVEGF-PEG-DOTA/⁶⁸Ga suggest that uptake of intravenously injected tracer in mouse tumors reaches plateau as early as 25 sec after injection, most likely through the first pass (82).

There are several variables that might affect accumulation of VEGF-based tracers in tumor endothelial cells, the prevalence of VEGF receptors in angiogenic vasculature, the rate of receptor-mediated internalization, and the levels (systemic or local) of endogenous VEGF. Another variable is the presence of VEGF receptors on tumor cells, which although not as

widespread as the presence of integrins, might still affect imaging results in some tumors.

Several groups described contrast agents based on anti-VEGFR antibodies, which were derivatized with IRD800 near-infrared fluorescent dye (89), coupled to ultrasound microbubbles (90-92), or coupled to ^{99m}Tc or Cy5.5-labeled chitosan-DC101 conjugates (93). Another emerging approach is to use VEGFR-binding peptides multiplexed on ultrasound microbubbles to enhance affinity to VEGF receptors (94-96). Finally, several small molecule VEGFR kinase inhibitors have been radiolabeled with ¹⁸F and ¹¹C for PET imaging (97-99) and, at least one of the resulting tracers demonstrated preferential accumulation at the outer rim of the tumor with a pattern of distribution which did not follow ¹⁸F-FDG uptake (98). Considering powerful techniques that are available for selection of high affinity peptides (100), various forms of antibodies, and new scaffolds with variable regions (e.g. adnectin, ref. 101), it would be natural to expect that new targeting moieties for imaging VEGF receptors would continue to be discovered.

VEGFR imaging and therapy monitoring. So far, there are only few publications that employed targeted VEGFR imaging in tumor treatment setting. In the first reported experiments, Cys-tagged VEGF₁₂₁ was site-specifically derivatized with HYNIC, radiolabeled with ^{99m}Tc and used as a SPECT tracer for imaging VEGFR in orthotopic 4T1 tumors in Balb/c mice subjected to chemotherapy with cyclophosphamide (78). Treatment with high dose regimen (CP at 150 mg/kg i.p. q.o.d., four total doses, n = 9) or low dose metronomic regimen (CP at 25 mg/kg i.p. q.d., seven total doses, n = 9) cause the same tumor growth inhibition and very similar decrease in tracer uptake in tumor vasculature. Interestingly, neither regimen significantly changed microvascular density, as judged by CD31 immunostaining, but both regimens depleted VEGFR-2 overexpressing endothelial cells from tumor vasculature, suggesting that such cells are primarily responsible for uptake of VEGF-based tracers.

As indicated above, Kiessling's group used ultrasound imaging with microbubbles driven by anti-VEGFR-2 antibody, to monitor the effects of the potent MMP inhibitor AG3340 (Prinomastat), using subcutaneous human squamous cell carcinoma HaCaT-ras-A-5RT3 grown in left hind leg of nude mice (44). In that model, drug-induced decrease in microvascular density was associated with upregulation of VEGFR-2 and therefore there were no statistically significant longitudinal changes in tracer binding in the course of treatment.

The effects of sunitinib on VEGFR imaging were explored in 4T1 mouse mammary breast carcinoma tumor grown in the right hind limb (89). In this model, 5-day sunitinib treatment inhibited tumor growth and caused a 40% decrease in the immunostaining of VEGFR-2 on tumor histological sections, although changes in microvascular density were not statistically significant, as judged by immunostaining for a pan-endothelial marker. To enable VEGFR imaging, commercially available anti-VEGFR-2 antibody (α VEGFR2ab) that was randomly derivatized with IRD800 near-infrared fluorescent dye and used for intravenous injections. The retention of NIR800- α VEGFR2ab in untreated tumors was 2.356 ± 0.074 (n = 10) higher than in the contralateral limb, while for treated animals this ratio was 1.832 ± 0.1284 (n = 9), suggesting a ~22% sunitinib-induced decrease in tracer uptake.

The effects of another inhibitor of VEGFR tyrosine kinase activity, PTK787 (vatalanib) on VEGFR imaging were tested in U-251 rat glioma model (88). At seven day after tumor implantation in the brain, treatment was given daily for 5 days, followed by a

2-day break, the next cycle of 5-day daily treatment, and then 3-day later either MRI imaging or SPECT imaging with ^{99m}Tc-HYNIC/VEGF-C tracer. Unexpectedly, such treatment regimen caused faster tumor growth, higher vascularization at the tumor periphery, and the higher uptake of VEGFR targeting SPECT tracer. Interestingly, Western blot analysis indicated that the overall levels of VEGFR-2 and VEGFR-3 were lower in treated vs. control tumors. The latter finding might indicate that the higher tracer uptake could be determined by "better" accessibility and/or internalization of VEGFR-2 and VEGFR-3 in tumors with drug-induced enhanced vascularization.

Two more detailed studies of the effects of tyrosine kinase inhibitors on imaging VEGFR prevalence revealed complex time-dependent patterns (85, 86). In both studies SPECT imaging of VEGFR with scVEGF/^{99m}Tc tracer (single-chain VEGF directly radiolabeled with ^{99m}Tc on Cys-tag) was coupled with immunohistochemical analysis of VEGFR-2 and a pan-endothelial marker CD31. Importantly, in vitro experiments indicated that tyrosine kinase inhibitors do not inhibit VEGFR-2 mediated uptake of scVEGF-based tracer, allowing for imaging treated animals (85, 86). In one study (85), VEGFR was imaged in subcutaneous HT29 xenografts in nude mice treated with pazopanib, an FDA-approved small molecule tyrosine kinase inhibitor targeting VEGFR, PDGFR and c-Kit (102, 103). In this model, SPECT imaging and autoradiography of tumor cryosections indicated that scVEGF/^{99m}Tc tracer accumulated preferentially at the tumor periphery (Fig. 6). Although tumor growth was barely affected by Day 5 of treatment, non-invasive VEGFR-2 imaging revealed early, rather dramatic effects of pazopanib on tumor vasculature. SPECT imaging and autoradiography of tumor sections indicated that 5-day pazopanib treatment resulted in ~3-fold decrease in tracer uptake and immunohistochemical analysis established a corresponding decrease in the number of CD31⁺/VEGFR-2⁺ endothelial cells on tumor sections. However, by Day 15 of continuous pazopanib treatment, the tracer uptake at the tumor periphery was significantly increased relatively 5-day time point, while immunohistochemical analysis indicated re-growth of tumor vasculature with CD31⁺/VEGFR-2⁺ endothelial cells at the same peripheral regions. Importantly, these effects were observed despite 2-fold inhibition of tumor growth.

In another study, SPECT imaging with scVEGF/^{99m}Tc was used to explore the effects of sunitinib on the vasculature of orthotopic MDA231luc (luciferase-expressing derivative of human MDA-MB-231 breast carcinoma cells) tumors in nude

mice (86). Imaging with scVEGF/^{99m}Tc and autoradiography of tumor cryosections revealed a 2.2- to 2.6-fold decrease in tracer uptake after four daily doses of sunitinib. However, once treatment was discontinued, tracer uptake rapidly (3 days) increased, particularly at the tumor edges. Immunohistochemical analysis of VEGFR-2 and CD31 supported imaging findings, revealing the corresponding depletion of VEGFR-2⁺/CD31⁺ endothelial cells from tumor vasculature during the course of treatment, as well as rapid re-emergence of VEGFR-2⁺/CD31⁺ vasculature at the tumor edges after discontinuation of treatment. Interestingly, resuming sunitinib treatment after the 3-day break caused vascular regression in some, but not all mice, suggesting that resistance to sunitinib might emerge quite rapidly. Of note, similar pattern of vascular regression and rebound after treatment with sunitinib was reported in A2780 and Colo205 tumor models, using PET imaging with ⁸⁹Zr-ranibizumab, a tracer based on ranibizumab, a monoclonal antibody fragment (Fab) derivative of VEGF-neutralizing bevacizumab, which is currently used to treat macular degeneration, and whose accumulation in tumor reflects combination of vascular perfusion and VEGF presence in the tumor tissue (104).

Taken together, initial experience with imaging VEGF receptors in the course of treatment indicates that changes in their prevalence can be detected in the course of vascular regression and, critically, vascular rebound associated with emergence of drug-resistant vasculature. Somewhat surprisingly, despite continuous treatment with VEGFR tyrosine kinase inhibitors (e.g. pazopanib, sunitinib, vatalanib), drug-resistant vasculature still populated by endothelial cells overexpressing VEGFR-2, and receptor-mediated endocytosis continues to accumulate VEGF-tracers inside the targeted cells.

As noted at the beginning of this review, the mechanisms of action of anti-angiogenic drugs that target the VEGF/VEGFR pathway as well as mechanisms of resistance to such drugs are not fully understood (1-10). These drugs, which include inhibitors of VEGFR kinase activity and biologics that either block VEGF receptors or sequester VEGF, are not cytotoxic or even cytostatic. The emerging consensus is that in tumor microenvironment these drugs induce transient regression of tumor vasculature through yet unknown mechanisms, followed by "adaptive-invasive" revascularization or vascular rebound, which may lead to enhanced invasiveness and metastatic dissemination of the tumor (105, Fig. 7). The timing, magnitude, and significance of vascular regression and revascularization are critical for development of

treatment regimens. For example, regression might involve so-called "normalization" of tumor vasculature (106, 107), which might provide for a better delivery of chemotherapeutic drugs to tumor growth areas. In turn, revascularization might also provide for better drug delivery, justifying the combination regimens and particularly metronomic combinations (108). On the other hand, recent research in mouse tumor models suggested that revascularization might stimulate invasiveness and metastatic dissemination of primary tumor (105, 109). In view of these complexities, there is an urgent and still unmet need in developing predictive biomarkers suitable for analysis of different stages in the course of VEGF/VEGFR-directed therapies (110). Since vascular regression and rebound are associated with the complex dynamic changes in the prevalence of the drug target itself, it is tempting to speculate that non-invasive molecular imaging of VEGF receptors would be able to satisfy this need. If responses of human vasculature follow the same pattern of vascular regression and rebound, longitudinal VEGFR imaging could be able to detect patients who respond to therapy at the early stage of treatment and then identify those patients whose VEGFR-2 expressing vasculature stop responding and who would benefit if treatment is changed.

Clinical trials with tracers for imaging VEGF receptors. To the best of our knowledge there are no publications on Phase I/II clinical trials for VEGFR imaging tracers. However in 2003 and 2004, Li et al published two reports on using imaging with ¹²³I-VEGF₁₆₅ in patients with gastrointestinal tumors (66, 67). Intravenous injection of ~5 µg of tracer was well-tolerated without detectable side effects and rather heterogeneous tracer accumulation in tumor and metastasis was imaged at 30 min post-injection in 18 patients (66). Using CT and MRI data as a "gold standard", in patients with pancreatic adenocarcinomas, primary tumors were visualized in seven of nine, lymph node metastases in three of four, liver metastases in three of six and lung metastases in one of three. Cholangiocarcinomas were visualized by ¹²³I-VEGF₁₆₅ imaging in one of two patients. Hepatocellular carcinomas were visible in two of four patients. Weakly positive scans were registered in one patient with abdominal schwannoma and in one patient with peritoneal carcinosis. Of note, the majority of false-negative results were obtained in patients with tumors and metastases with maximum median diameter of <2 cm. In a follow up studies in 9 patients with pancreatic carcinoma, majority of primary pancreatic tumors and their metastases was visualized using ¹²³I-VEGF₁₆₅ tracer (67).

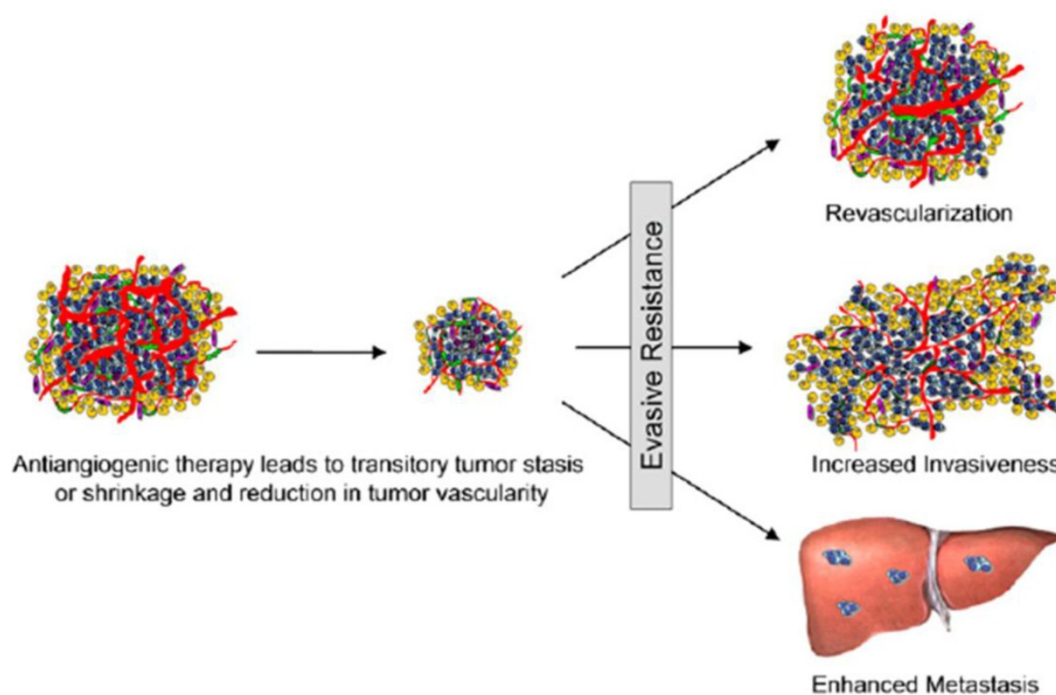


Figure 7. Adaptive-Evasive Responses by Tumors to Antiangiogenic Therapies (105). Schematic summary of adaptive responses to VEGF/VEGFR inhibitors (and likely other angiogenesis inhibitors) that elicit “evasive resistance.” Tumors respond to VEGF/VEGFR pathway inhibition with tumor stasis or regression and a loss of blood vessels, but mechanisms of evasive resistance to the antiangiogenic treatment are then induced that can variously enable revascularization via alternative proangiogenic signals, increased local invasiveness, and/or enhanced distant metastasis.

Conclusions

Currently, targeted tracers for molecular imaging of integrins and VEGF receptors in different modalities receptors are reasonable well-developed and some RGD-based tracers are already in clinical trials. Only extensive clinical trials can establish whether imaging with these molecular tracers would be able to compete with MRI, CT, or metabolic PET imaging in detection and staging of primary tumors and metastatic lesions. More promising might be application of molecular imaging for image-guided therapy, whereby the effects of drugs, particularly drugs that specifically targeting integrins, VEGF receptors, or other targets in angiogenic vasculature, are evaluated in real time in individual patients. Certainly, this strategy would require extensive clinical trials and multi-disciplinary collaborations; however considering ever growing demand for personalized yet not too expensive medicine, this strategy might respond to unmet medical needs.

Acknowledgements

This work was supported by NIH grant 2 R44 CA141806-02A1 to JMB.

Competing Interests

J. Backer is a shareholder in SibTech, Inc.

References

1. Bussolati B, Grange C, Camussi G. Tumor exploits alternative strategies to achieve vascularization. *FASEB J.* 2011; 25:2874-82.
2. Leite de Oliveira R, Hamm A, Mazzone M. Growing tumor vessels: more than one way to skin a cat - implications for angiogenesis targeted cancer therapies. *Mol Aspect Medicine.* 2011; 32: 71-87.
3. Potente M, Gerhardt H, Carmeliet P. Basic and therapeutic aspects of angiogenesis. *Cell.* 2011; 146: 873-87.
4. Bergers G, Hanahan D. Modes of resistance to antiangiogenic therapy. *Nature Rev Cancer.* 2008; 8: 592-603.
5. Crawford Y, Ferrara N. Tumor and stromal pathways mediating refractoriness/resistance to anti-angiogenic therapies. *Trend Pharmacol Sci.* 2009; 30: 624-30.
6. Azam F, Mehta S, Harris AL. Mechanisms of resistance to antiangiogenesis therapy. *Eur J Cancer.* 2010; 46: 1323-32.
7. Bridges EM, Harris AL. The angiogenic process as a therapeutic target in cancer. *Biochemical Pharmacology.* 2011; 81: 1183-91.
8. Sharma PS, Sharma R, Tyagi T. VEGF/VEGFR pathway inhibitors as anti-angiogenic agents: present and future. *Curr Cancer Drug Target.* 2011; 11: 624-53.
9. Ribatti D. Novel angiogenesis inhibitors: addressing the issue of redundancy in the angiogenic signaling pathway. *Cancer Treat Rev.* 2011; 37: 344-52.
10. Avraamides CJ, Garmy-Susini B, Varner JA. Integrins in angiogenesis and lymphangiogenesis. *Nature Rev Cancer.* 2008; 8: 604-17.
11. Legate KR, Montañez E, Kudlacek O, Füssler R, ILK, PINCH and parvin: the tHPP of integrin signaling. *Nature Rev Mol Cell Biol.* 2006; 7: 20-31.
12. Beer AJ, Schwaiger M. Imaging of integrin alphavbeta3 expression. *Cancer Met Rev.* 2008; 27: 631-44.

13. Tugues S, Koch S, Gualandi L, et al. Vascular endothelial growth factors and receptors: anti-angiogenic therapy in the treatment of cancer. *Mol Aspect Med.* 2011; 32: 88-111.
14. Koch S, Tugues S, Li X, et al. Signal transduction by vascular endothelial growth factor receptors. *Biochem J.* 2011; 437: 169-83.
15. Ferrara N. VEGF-A: a critical regulator of blood vessel growth. *Eur Cytokine Network.* 2009; 20: 158-63.
16. Schliemann C, Neri D. Antibody-based vascular tumor targeting. *Recent Res Cancer Res.* 2010;180: 201-16.
17. Laakkonen P, Vuorinen K. Homing peptides as targeted delivery vehicles. *Integr Biol Quant Biosci Nano Macro.* 2010; 2: 326-37.
18. Haubner R, Wester HJ, Reuning U, et al. Radiolabeled alpha(v)beta3 integrin antagonists: a new class of tracers for tumor targeting. *J Nucl Med* 1999; 40: 1061-71.
19. Schottelius M, Laufer B, Kessler H, Wester HJ. Ligands for mapping alphavbeta3-integrin expression in vivo. *Acc Chem Res.* 2009; 42: 969-80.
20. Dijkgraaf I, Beer AJ, Wester HJ. Application of RGD-containing peptides as imaging probes for alphavbeta3 expression. *Front Biosci.* 2009; 14: 887-99.
21. Pan D, Pramanik M, Senpan A, et al. Molecular photoacoustic imaging of angiogenesis with integrin-targeted gold nanobeacons. *FASEB J.* 2011; 25: 875-82.
22. Anderson CR, Hu X, Zhang H, et al. Ultrasound molecular imaging of tumor angiogenesis with an integrin targeted microbubble contrast agent. *Invest Radiol.* 2011; 46: 215-24.
23. Thumshirn G, Hersel U, Goodman SL, Kessler H. Multimeric cyclic RGD peptides as potential tools for tumor targeting: Solid-phase peptide synthesis and chemoselective oxime ligation. *Chem.* 2003; 9: 2717-25.
24. Poethko T, Schottelius M, Thumshirn G, et al. Two-step methodology for high-yield routine radiohalogenation of peptides: 18F-labeled RGD and octreotide analogs. *J Nucl Med* 2004; 45: 892-902.
25. Poethko T, Schottelius M, Thumshirn G, et al. Chemoselective pre-conjugate radiohalogenation of unprotected mono- and multimeric peptides via oxime formation. *Radiochim Acta,* 2004; 92: 317-27.
26. Liu S, Hsieh WY, Jiang Y, et al. Evaluation of a (99m)Tc-labeled cyclic RGD tetramer for noninvasive imaging integrin alpha(v)beta3-positive breast cancer. *Bioconjug Chem* 2007; 18: 438-46.
27. Li ZB, Cai W, Cao Q, et al. (64)Cu-labeled tetrameric and octameric RGD peptides for small-animal PET of tumor alpha(v)beta(3) integrin expression. *J Nucl Med* 2007; 48: 1162-71.
28. Liu Z, Liu S, Wang F, Chen X. Noninvasive imaging of tumor integrin expression using (18F)-labeled RGD dimer peptide with PEG(4) linkers. *Eur J Nucl Med Mol Imaging* 2009; 36: 1296-307.
29. Sancey L, Garanger E, Foillard S, et al. Clustering and internalization of integrin alphavbeta3 with a tetrameric RGD-synthetic peptide. *Mol Ther J Am Soc Gene Ther.* 2009; 17: 837-43.
30. Mulder WJ, Castermans K, van Beijnum JR, et al. Molecular imaging of tumor angiogenesis using alphavbeta3-integrin targeted multimodal quantum dots. *Angiogenesis.* 2009; 12: 17-24.
31. Kessinger CW, Khemtong C, Togo O, et al. In vivo angiogenesis imaging of solid tumors by alpha(v)beta(3)-targeted, dual-modality micellar nanoprobe. *Exp Biol Med.* 2010; 235: 957-65.
32. Chen W, Jarzyna PA, van Tilborg GA, et al. RGD peptide functionalized and reconstituted high-density lipoprotein nanoparticles as a versatile and multimodal tumor targeting molecular imaging probe. *FASEB J.* 2010; 24: 1689-99.
33. Akers WJ, Zhang Z, Berezin M, et al. Targeting of alpha(nu)beta(3)-integrins expressed on tumor tissue and neovasculature using fluorescent small molecules and nanoparticles. *Nanomed.* 2010; 5: 715-26.
34. Goutayer M, Dufort S, Josserand V, et al. Tumor targeting of functionalized lipid nanoparticles: assessment by in vivo fluorescence imaging. *Eur J Pharm Biopharm.* 2010; 75: 137-47.
35. Yang X, Hong H, Grailler JJ, et al. cRGD-functionalized, DOX-conjugated, and 64Cu-labeled superparamagnetic iron oxide nanoparticles for targeted anticancer drug delivery and PET/MR imaging. *Biomater.* 2011; 32: 4151-60.
36. Edwards WB, Akers WJ, Ye Y, et al. Multimodal imaging of integrin receptor-positive tumors by bioluminescence, fluorescence, gamma scintigraphy, and single-photon emission computed tomography using a cyclic RGD peptide labeled with a near-infrared fluorescent dye and a radionuclide. *Mol Imag.* 2009; 8: 101-10.
37. Yu MK, Park J, Jeong YY, et al. Integrin-targeting thermally cross-linked superparamagnetic iron oxide nanoparticles for combined cancer imaging and drug delivery. *Nanotech.* 2010; 21: 415102.
38. Garanger E, Boturn D, Dumy P. Tumor targeting with RGD peptide ligands-design of new molecular conjugates for imaging and therapy of cancers. *Curr Med Chem Anti-Cancer Agents.* 2007; 7: 552-8.
39. Xie H, Diagaradjane P, Deorukhkar AA, et al. Integrin alphavbeta3-targeted gold nanoshells augment tumor vasculature-specific imaging and therapy. *Int J Nanomed.* 2011; 6: 259-69.
40. Ferl GZ, Dumont RA, Hildebrandt JJ, et al. Derivation of a compartmental model for quantifying 64Cu-DOTA-RGD kinetics in tumor-bearing mice. *J Nucl Med* 2009; 50: 250-8.
41. Jin ZH, Razkin J, Josserand V, et al. In vivo noninvasive optical imaging of receptor-mediated RGD internalization using self-quenched Cy5-labeled RAFT-c(-RGDfK-)(4). *Mol Imag.* 2007; 6: 43-55.
42. Reynolds AR, Hart IR, Watson AR, et al. Stimulation of tumor growth and angiogenesis by low concentrations of RGD-mimetic integrin inhibitors. *Nature Med.* 2009; 15: 392-400.
43. Jung KH, Lee KH, Paik JY, et al. Favorable biokinetic and tumor-targeting properties of 99mTc-labeled glucosamine RGD and effect of paclitaxel therapy. *J Nucl Med.* 2006; 47: 2000-7.
44. Palmowski M, Huppert J, Ladewig G, et al. Molecular profiling of angiogenesis with targeted ultrasound imaging: early assessment of antiangiogenic therapy effects. *Mol Cancer Ther.* 2008; 7: 101-9.
45. Palmowski M, Peschke P, Huppert J, et al. Molecular ultrasound imaging of early vascular response in prostate tumors irradiated with carbon ions. *Neoplasia.* 2009; 11: 856-63.
46. Morrison MS, Ricketts SA, Barnett J, et al. Use of a novel Arg-Gly-Asp radioligand, 18F-AH111585, to determine changes in tumor vascularity after antitumor therapy. *J Nucl Med.* 2009; 50: 116-22.
47. Battle MR, Goggi JL, Allen L, et al. Monitoring tumor response to antiangiogenic sunitinib therapy with 18F-Fluciclatide, an 18F-labeled and alpha;V[beta]3-integrin and alpha;V[beta]5-integrin imaging agent. *J Nucl Med* 2011; 52: 424-430.
48. Indrevoll B, Kindberg GM, Solbakken M, et al. NC-100717: a versatile RGD peptide scaffold for angiogenesis imaging. *Bioorg Med Chem Lett.* 2006; 16: 6190-3.
49. Dumont RA, Hildebrandt I, Su H, et al. Noninvasive imaging of alphaVbeta3 function as a predictor of the antimigratory and antiproliferative effects of dasatinib. *Cancer Res.* 2009; 69: 3173-9.
50. Yang M, Gao H, Yan Y, et al. PET imaging of early response to the tyrosine kinase inhibitor ZD4190. *Eur J Nucl Med Mol Imaging.* 2011; 38: 1237-47.
51. Haubner R, Weber WA, Beer AJ, et al. Noninvasive visualization of the activated avh3 integrin in cancer patients by positron emission tomography and [18F]galacto- RGD. *PLoS Med* 2005; 2:e70.
52. Beer AJ, Haubner R, Goebel M, et al. Biodistribution and pharmacokinetics of the avβ3 selective tracer 18F Galacto-RGD in cancer patients. *J Nucl Med.* 2005; 46: 1333-41.
53. Beer AJ, Haubner R, Sarbia M, et al. Positron emission tomography using [18F]galacto-RGD identifies the level of integrin avh3 expression in man. *Clin Cancer Res* 2006; 12:3942-9.
54. Beer AJ, Haubner R, Wolf I, et al. PET-based human dosimetry of 18F-galacto- RGD, a new radiotracer for imaging avβ3 expression. *J Nucl Med.* 2006; 47: 763-9.
55. Beer AJ, Grosu AL, Carlsen J, et al. [18F]galacto-RGD positron emission tomography for imaging of avb3 expression on the neovasculature in patients with squamous cell carcinoma of the head and neck. *Clin Cancer Res.* 2007; 13: 6610-16.
56. Beer AJ, Niemeier M, Carlsen J, et al. Comparison of integrin alphavbeta3 expression and glucose metabolism in primary and metastatic lesions in cancer patients: a PET study using 18F-galacto-RGD and 18F-FDG. *J Nucl Med.* 2008; 49:22-9.
57. Beer AJ, Niemeier M, Carlsen J, et al. Patterns of alphavbeta3 expression in primary and metastatic human breast cancer as shown by 18F-Galacto-RGD PET. *J Nucl Med.* 2008; 49: 255-9.
58. Schnell O, Krebs B, Carlsen J, et al. Imaging of integrin alpha(v)beta(3) expression in patients with malignant glioma by [18F] Galacto-RGD positron emission tomography. *Neuro-Oncology.* 2009; 11: 861-70.
59. Bach-Gansmo T, Danielsson R, Saracco A, et al. (2006). Integrin receptor imaging of breast cancer: A proof-of-concept study to evaluate 99mTc-NC100692. *J Nucl Med.* 2006; 47: 1434-39.
60. Bach-Gansmo T, Skretting A, Bogsrud TV. Integrin scintimammography using a dedicated breast imaging, solid-state gamma-camera and 99mTc-labelled NC100692. *Clin Phys Funct Imag.* 2008; 28: 235-9.
61. Axelsson R, Bach-Gansmo T, Castell-Conesa J, McParland BJ, Study Group. An open-label, multicenter, phase 2a study to assess the feasibility of imaging metastases in late-stage cancer patients with the alpha v beta 3-selective angiogenesis imaging agent 99mTc-NC100692. *Acta Radiologica.* 2010; 51: 40-6.

62. Kenny LM, Coombes RC, Oulie I, et al. Phase I trial of the positron-emitting Arg-Gly-Asp (RGD) peptide radioligand 18F-AH111585 in breast cancer patients. *J Nucl Med.* 2008; 49: 879-86.
63. Mittra ES, Goris ML, Iagaru AH, et al. Pilot pharmacokinetic and dosimetric studies of (18)F-FPPRGD2: a PET radiopharmaceutical agent for imaging alpha(v)beta(3) integrin levels. *Radiol.* 2011; 260: 182-91.
64. Cornelissen B, Oltenfreiter R, Kersemans V, et al. In vitro and in vivo evaluation of [123I]-VEGF165 as a potential tumor marker. *Nucl Med Biol.* 2005; 32: 431-6.
65. Yoshimoto M, Kinuya S, Kawashima A, et al. Radioiodinated VEGF to image tumor angiogenesis in a LS180 tumor xenograft model. *Nucl Med Biol.* 2006; 33: 963-9.
66. Li S, Peck-Radosavljevic M, Kienast O, et al. Imaging gastrointestinal tumours using vascular endothelial growth factor-165 (VEGF165) receptor scintigraphy. *Annal Oncol.* 2003; 14: 1274-77.
67. Li S, Peck-Radosavljevic M, Kienast O, et al. Iodine-123-vascular endothelial growth factor-165 (123I-VEGF165). Biodistribution, safety and radiation dosimetry in patients with pancreatic carcinoma. *Q J Nucl Med Mol Imag.* 2004; 48: 198-206.
68. Cai W, Chen K, Mohamedali KA, et al. PET of vascular endothelial growth factor receptor expression. *J Nucl Med.* 2006; 47: 2048-2056.
69. Wang H, Cai W, Chen K, et al. A new PET tracer specific for vascular endothelial growth factor receptor. *Eur J Nucl Med Mol Imag.* 2007; 34: 2001-10.
70. Cai W, Chen X. Multimodality imaging of vascular endothelial growth factor and vascular endothelial growth factor receptor expression. *Front Biosci.* 2007; 12: 4267-79.
71. Cai W, Guzman R, Hsu AR, et al. Positron emission tomography imaging of poststroke angiogenesis. *Stroke.* 2009; 40: 270-7.
72. Chen K, Cai W, Li ZB, et al. Quantitative PET imaging of VEGF receptor expression. *Mol Imag Biol.* 2009; 11: 15-22.
73. Chen K, Li ZB, Wang H, et al. Dual-modality optical and positron emission tomography imaging of vascular endothelial growth factor receptor on tumor vasculature using quantum dots. *Eur J Nucl Med Mol Imag.* 2008; 35: 2235-44.
74. Lu E, Wagner WR, Schellenberger U, et al. Targeted in vivo labeling of receptors for vascular endothelial growth factor: approach to identification of ischemic tissue. *Circulation* 2003; 108: 97-103.
75. Chan C, Sandhu J, Guha A, et al. A human transferrin(hnTf)-VEGF fusion protein containing an integrated binding site for ¹¹¹In for imaging tumor angiogenesis. *J Nucl Med* 2005; 46: 1745-52.
76. Wang H, Chen K, Niu G, Chen X. Site-specifically biotinylated VEGF(121) for near-infrared fluorescence imaging of tumor angiogenesis. *Mol Pharmacol.* 2009; 6: 285-94.
77. Backer MV, Gaynutdinov TI, Patel V, et al. Vascular endothelial growth factor selectively targets boronated dendrimers to tumor vasculature. *Mol Cancer Ther.* 2005; 4: 1423-9.
78. Blankenberg FG, Backer MV, Levashova Z, et al. In vivo tumor angiogenesis imaging with site-specific labeled (99m)Tc-HYNIC-VEGF. *Eur J Nucl Med Mol Imaging* 2006; 33: 841-48.
79. Backer MV, Levashova Z, Patel V, et al. Molecular imaging of VEGF receptors in angiogenic vasculature with single-chain VEGF-based probes. *Nature Med.* 2007; 13: 504-9.
80. Backer MV, Levashova Z, Levenson R, et al. Cysteine-containing fusion tag for site-specific conjugation of therapeutic and imaging agents to targeting proteins. *Methods Mol Biol.* 2008; 494: 275-94.
81. Eder M, Krivoshein AV, Backer M, et al. ScVEGF-PEG-HBED-CC and scVEGF-PEG-NOTA conjugates: comparison of easy-to-label recombinant proteins for [68Ga]PET imaging of VEGF receptors in angiogenic vasculature. *Nucl Med Biol.* 2010; 37: 405-12.
82. Blom E, Velikyan I, Monazzam A, et al. Synthesis and characterization of scVEGF-PEG-[68Ga]NOTA and scVEGF-PEG-[68Ga]DOTA PET tracers. *J Labl Compd Radiopharm.* 2011; [Epub ahead of print]
83. Levashova Z, Backer M, Backer JM, Blankenberg FG. Direct site-specific labeling of the Cys-tag moiety in scVEGF with technetium 99m. *Bioconjug Chem.* 2008; 19: 1049-54.
84. Anderson CR, Rychak JJ, Backer M, et al. scVEGF microbubble ultrasound contrast agents: a novel probe for ultrasound molecular imaging of tumor angiogenesis. *Invst Radiol.* 2010; 45: 579-85.
85. Blankenberg FG, Levashova Z, Sarkar SK et al. Noninvasive assessment of tumor VEGF receptors in response to treatment with pazopanib: a molecular imaging study. *Transl Oncol.* 2010; 3: 56-64.
86. Levashova Z, Backer M, Hamby CV, et al. Molecular imaging of changes in the prevalence of vascular endothelial growth factor receptor in sunitinib-treated murine mammary tumors. *J Nucl Med.* 2010; 51: 959-66.
87. Blankenberg FG, Levashova Z, Goris MG, et al. Targeted systemic radiotherapy with scVEGF/¹⁷⁷Lu leads to sustained disruption of the tumor vasculature and intratumoral apoptosis. *J Nucl Med.* 2011; 52: 1630-37.
88. Ali MM, Janic B, Babajani-Feremi A, et al. Changes in vascular permeability and expression of different angiogenic factors following anti-angiogenic treatment in rat glioma. *PLoS ONE* 2010; 5(1): e8727.
89. Virostko J, Xie J, Hallahan DE, et al. A molecular imaging paradigm to rapidly profile response to angiogenesis-directed therapy in small animals. *Mol Imag Biol.* 2009; 11: 204-12.
90. Rychak JJ, Graba J, Cheung AM, et al. Microultrasound molecular imaging of vascular endothelial growth factor receptor 2 in a mouse model of tumor angiogenesis. *Mol Imag.* 2007; 6: 289-96.
91. Liu H, Wang X, Tan KB, et al. Molecular imaging of vulnerable plaques in rabbits using contrast-enhanced ultrasound targeting to vascular endothelial growth factor receptor-2. *J Clin Ultrasound.* 2011; 39: 83-90.
92. Deshpande N, Ren Y, Foygel K, et al. Tumor angiogenic marker expression levels during tumor growth: longitudinal assessment with molecularly targeted microbubbles and US imaging. *Radiol.* 2011; 258: 804-11.
93. Lee CM, Kim EM, Cheong SJ, et al. Targeted molecular imaging of VEGF receptors overexpressed in ischemic microvasculature using chitosan-DC101 conjugates. *J Biomed Materials Res. Part A.* 2010; 92: 1510-7.
94. Brunel FM, Lewis JD, Destito G, et al. Hydrazine ligation strategy to assemble multifunctional viral nanoparticles for cell imaging and tumor targeting. *Nano Lett.* 2010; 10: 1093-7.
95. Tardy I, Pochon S, Theraulaz M, et al. Ultrasound molecular imaging of VEGFR2 in a rat prostate tumor model using BR55. *Inv Radiol.* 2010; 45: 573-8.
96. Pochon S, Tardy I, Bussat P, et al. BR55: a lipopeptide-based VEGFR2-targeted ultrasound contrast agent for molecular imaging of angiogenesis. *Inv Radiol.* 2010; 45: 89-95.
97. Ilovich O, Jacobson O, Aviv Y, et al. Formation of fluorine-18 labeled diaryl ureas--labeled VEGFR-2/PDGFR dual inhibitors as molecular imaging agents for angiogenesis. *Bioorg Med Chem.* 2008; 16: 4242-51.
98. Samen E, Thorell JO, Lu L, et al. Synthesis and preclinical evaluation of [(11)C]PAQ as a PET imaging tracer for VEGFR-2. *Eur J Nucl Med Mol Imag.* 2009; 36:1283-95.
99. Gao M, Lola CM, Wang M, et al. Radiosynthesis of [(11)C]vandetanib and [(11)C]chloro-vandetanib as new potential PET agents for imaging of VEGFR in cancer. *Bioorg Med Chem Lett.* 2011; 21: 3222-6.
100. Gautier B, Goncalves V, Diana D, et al. Biochemical and structural analysis of the binding determinants of a vascular endothelial growth factor receptor peptidic antagonist. *J Med Chem.* 2010; 53: 4428-40.
101. Dineen SP, Sullivan LA, Beck AW, et al. The Adnectin CT-322 is a novel VEGF receptor 2 inhibitor that decreases tumor burden in an orthotopic mouse model of pancreatic cancer. *BMC Cancer.* 2008; 8: 352.
102. Kumar R, Knick VB, Rudolph SK, et al. Pharmacokinetic-pharmacodynamic correlation from mouse to human with pazopanib, a multikinase angiogenesis inhibitor with potent antitumor and antiangiogenic activity. *Mol. Cancer Ther.* 2007; 6: 2012-21.
103. Schutz FA, Choueiri TK, Sternberg CN. Pazopanib: Clinical development of a potent anti-angiogenic drug. *Crit Rev Oncol-Hematol.* 2011; 77: 163-71.
104. Nagengast WB, Lub-de Hooge MN, Oosting SF, et al. VEGF-PET imaging is a noninvasive biomarker showing differential changes in the tumor during sunitinib treatment. *Cancer Res.* 2011; 71: 143-53.
105. Paez-Ribes M, Allen E, Hudock J, et al. Antiangiogenic therapy elicits malignant progression of tumors to increased local invasion and distant metastasis. *Cancer Cell.* 2009; 15: 220-31.
106. Goel S, Duda DG, Xu L, et al. Normalization of the vasculature for treatment of cancer and other diseases. *Physiol Rev.* 2011; 91: 1071-121.
107. De Bock K, Cauwenberghs S, Carmeliet P. Vessel abnormalization: another hallmark of cancer? Molecular mechanisms and therapeutic implications. *Curr Opin Gen Dev.* 2011; 21: 73-9.
108. Pasquier E, Kavallaris M, Andre N. Metronomic chemotherapy: new rationale for new directions. *Nature Rev Clin Oncol.* 2010; 7: 455-65.
109. Ebos JM, Lee CR, Cruz-Munoz W, et al. Accelerated metastasis after short-term treatment with a potent inhibitor of tumor angiogenesis. *Cancer Cell.* 2009; 15: 232-39.
110. Gerger A, LaBonte M, Lenz HJ. Molecular predictors of response to antiangiogenesis therapies. *Cancer J.* 2011; 17: 134-41.